Vol. 86: 29–46, 2021
https://doi.org/10.3354/ame01955

AQUATIC MICROBIAL ECOLOGY
Aquat Microb Ecol

Published online February 25

A phosphate starvation response gene (*psr*1-like) is present and expressed in *Micromonas pusilla* and other marine algae

Cara L. Fiore[1,3,*], Harriet Alexander[2,4], Melissa C. Kido Soule[1], Elizabeth B. Kujawinski[1]

[1]Department of Marine Chemistry and Geochemistry, Woods Hole Oceanographic Institution, Woods Hole, MA 02543, USA
[2]MIT/WHOI Joint Program in Oceanography and Applied Ocean Sciences, Department of Biology, Woods Hole Oceanographic Institution, Woods Hole, MA 02543, USA
[3]*Present address:* Biology Department, Appalachian State University, Boone, NC 28608, USA
[4]*Present address:* Department of Biology, Woods Hole Oceanographic Institution, Woods Hole, MA 02543, USA

ABSTRACT: Phosphorus (P) limits primary production in regions of the surface ocean, and many plankton species exhibit specific physiological responses to P deficiency. The metabolic response of *Micromonas pusilla*, an ecologically relevant marine photoautotroph, to P deficiency was investigated using metabolomics and comparative genomics. The concentrations of some intracellular metabolites were elevated in the P-deficient cells (e.g. xanthine, inosine), and genes involved in the associated metabolic pathways shared a predicted conserved amino acid motif in the non-coding regions of each gene. The presence of the conserved motif suggests that these genes may be co-regulated, and the motif may constitute a regulatory element for binding a transcription factor, specifically that of Psr1 (phosphate starvation response). A putative phosphate starvation response gene (*psr*1-like) was identified in *M. pusilla* with homology to well characterized *psr*1/*phr*1 genes in algae and plants, respectively. This gene appears to be present and expressed in other marine algal taxa (e.g. *Emiliania huxleyi*) in field sites that are chronically P limited. Results from the present study have implications for understanding phytoplankton taxon-specific roles in mediating P cycling in the ocean.

KEY WORDS: *Micromonas pusilla* · Phosphate stress response · Marine algae · Metabolomics · Dissolved organic matter · Biological oceanography

1. INTRODUCTION

Phosphorus (P) is a critical element for life, and is found in lipid membranes, genetic material, and energy storage compounds. Because most marine microorganisms preferentially take up P as inorganic phosphate (PO_4^{3-}), concentrations of dissolved inorganic P are generally below 1 µM in the surface ocean (Karl 2014), which limits phytoplankton productivity (Tyrrell 1999).

Marine phytoplankton respond to chronic P deficiency by investing resources in P uptake via inorganic and organic compounds (Chung et al. 2003, Lin et al. 2016, Sosa et al. 2019), remodeling cellular metabolism and structures (Berdalet et al. 1994, Van Mooy et al. 2009, Martin et al. 2011, Shemi et al. 2016, Cañavate et al. 2017, Kujawinski et al. 2017), and storing P (Dyhrman et al. 2012, Martin et al. 2014). Different mechanisms for enacting these responses have evolved in widely distributed and often sympatric phytoplankton taxa. For example, within the diatom *Phaeodactylum tricornutum*, proteomics indicated broadly depressed metabolic activity as a

*Corresponding author: fiorec@appstate.edu

Publisher: Inter-Research · www.int-res.com

response to P starvation (Feng et al. 2015). Specifically, energy metabolism, amino acid metabolism, nucleic acid metabolism, and photosynthesis were down-regulated, while protein degradation, lipid accumulation, and photorespiration were up-regulated (Feng et al. 2015). In contrast, the prymnesiophytes *Prymnesium parvum* and *Emiliania huxleyi* and the dinoflagellates *Prorocentrum donghaiense* and *Amphidinium carterae* maintained energy-generating processes (i.e. photosynthesis) and carbon fixation in response to P deficiency (Lai et al. 2011, Li et al. 2016, Rokitta et al. 2016, Shi et al. 2017). Interestingly, *P. donghaiense* increased nitrate assimilation under P deficiency (Shi et al. 2017), whereas *E. huxleyi* reduced nitrate uptake with a tight coupling between P and nitrogen (N) pools (Rokitta et al. 2016). While the experimental designs differ slightly across studies, the aggregate results indicate the presence of both taxon-specific differences and cross-taxon similarities in the physiological response of phytoplankton to P deficiency (Rengefors et al. 2003, Lomas et al. 2004, Lin et al. 2016, Martiny et al. 2020). These strategies all minimize non-critical P utilization and maximize P uptake, and thus play important roles in structuring phytoplankton assemblages in the oceans (Dyhrman & Ruttenberg 2006, Dyhrman et al. 2009, Martin et al. 2011, Rokitta et al. 2016, Guo et al. 2018).

The cosmopolitan picoeukaryotic groups *Micromonas* and *Ostreococcus* spp. are important marine primary producers (Li 1994). *Micromonas* spp. are of particular interest due to the abundance and wide distribution of organisms in this genus (Demory et al. 2017). Recent culture experiments with *M. pusilla* isolated from Svalbard (Hoppe et al. 2018) and *M. pusilla* Lac38 (Maat et al. 2014) also indicated that these strains are likely to be successful under conditions of increased acidification and low nutrient (P) availability. This success may be due, in part, to higher efficiency of carbon sequestration for growth under high pCO_2 conditions and/or the ability to remodel photosystem proteins under nutrient-limited conditions (Maat et al. 2014, Guo et al. 2018, Hoppe et al. 2018). Additionally, similar to other phytoplankton (Chung et al. 2003), *M. pusilla* may shift lipid composition to increase non-P-containing lipids (Maat et al. 2016, Guo et al. 2018), as well as up-regulate genes and proteins for inorganic and organic P transporters (Whitney & Lomas 2016, Guo et al. 2018) and for polyphosphate accumulation (Bachy et al. 2018). However, some of the broader physiological response mechanisms of *M. pusilla* and other prasinophytes to P deficiency have yet to be fully explored.

Micromonas species are part of the 'green' lineage (Chlorophyta) of organisms, a monophyletic group including land plants. Consequently, their physiological response to nutritional stressors, like P deficiency, may share more traits with land plants than with other algal groups (e.g. diatoms, haptophytes). Indeed, P deficiency is common in lakes and terrestrial systems (Elser et al. 2007). The physiological response of model chlorophytes such as the land plant *Arabidopsis thaliana* and the freshwater green alga *Chlamydomonas reinhardtii* to P deficiency led to the identification of a phosphate starvation response gene described as *psr*1 in *C. reinhardtii* (Wykoff et al. 1999) and as *phr*1 in plants (Rubio et al. 2001). This gene encodes for a transcription factor (TF), a protein that binds to specific DNA regions to activate or repress transcription of one or more genes. The specific region of DNA to which TFs bind is typically characterized by a short repetitive nucleotide sequence, or motif, found up- or downstream of a given gene or within introns (Barrett et al. 2012, Franco-Zorrilla et al. 2014). In *A. thaliana,* regulatory motifs for the Phr1 protein were more abundant in known P-responsive genes than in the rest of the genome (Müller et al. 2007), linking Phr1 to the regulation of P-responsive genes. Phr1/Psr1 TFs have not been described, to our knowledge, in marine algae.

Here, we use a combined metabolomic and comparative genomic approach to investigate the impact of P deficiency on the physiology of *M. pusilla* CCMP1545. Many metabolites are produced by metabolic pathways under genetic regulatory control (e.g. De Carvalho & Fernandes 2010, Markou & Nerantzis 2013); thus, our approach complements recent physiological, transcriptional, and proteomic work (Guo et al. 2018, Hoppe et al. 2018) and provides mechanistic insight into the physiological response to P deficiency and its underlying genetic regulation. We used a targeted metabolomics approach to analyze the suite of intracellular and extracellular molecules produced by *M. pusilla*. Informed by our metabolomics results, we employed a comparative genetics approach to identify (1) a *psr*1-like gene in *M. pusilla* and other prevalent marine phytoplankton species and (2) a potential DNA-binding site of the Psr1-like protein in putatively P-responsive genes. We found evidence for the expression of *psr*1-like genes in *M. pusilla* and other marine algae under P-deficient conditions in cultures and in the field. These results have implications for better understanding the metabolic response of diverse phytoplankton groups to P deficiency.

2. MATERIALS AND METHODS

2.1. Culture of *Micromonas pusilla* CCMP 1545

All glassware was acid-cleaned and combusted at 450°C for at least 4 h. We grew an axenic culture of *M. pusilla* CCMP1545 from the National Center for Marine Algae and Microbiota (Boothbay, ME, USA) in L1-Si media (https://ncma.bigelow.org/algal-media-recipes) with 0.2-µm filtered (Omnipore filters; Millipore) autoclaved seawater from Vineyard Sound (MA, USA). We maintained the cultures at 22°C under a 12:12 h light:dark regime (84 µmol photons m^{-2} s^{-1}). After acclimation to these culture conditions, we split the culture into 2 parallel cultures of L1-Si media amended with (a) 36 µM phosphate (P replete) or (b) 0.4 µM phosphate (P deficient). We maintained these parallel cultures for 3 generations prior to this experiment. At the start of the experiment, we inoculated 9 flasks of each media type with exponential-phase cells to achieve approximately 300 000 cells in each flask in 320 ml total volume (n = 3 per treatment for each time point). We also created 3 cell-free control flasks for each treatment. We grew cultures for 2 wk and sampled approximately 1 h into the light cycle at experiment initiation (T_0; Day 0), in late exponential growth phase (T_1; Day 4 P deficient; Day 6 P replete), and in stationary phase (T_2; Day 5 P deficient; Day 13 P replete) (Fig. S1 in Supplement 1 at www.int-res.com/articles/suppl/a086p029_supp1.pdf).

At each sampling point, we removed 1 ml for cell counts and chlorophyll fluorescence, 30 ml for total organic carbon (Text S1 in Supplement 1), and 20 ml of filtrate (see section 2.2) for nutrients. We monitored cell abundance daily by flow cytometry (Guava, Millipore) and assessed Photosystem II efficiency by measuring the variable and maximum chlorophyll fluorescence (F_v/F_m) using fluorescence induction and relaxation (Satlantic). We used chlorophyll *a* (692 nm) and side scatter of *M. pusilla* cultures to optimize flow cytometry settings. We assessed potential bacterial contamination by viewing DAPI-stained cells at each time point (Text S1).

2.2. Metabolite extraction and instrument methods

Metabolite extraction and analytical methods were optimized for semi-polar compounds with a size range of 100–1000 Da, capturing many primary metabolites such as organic acids, vitamins, and nucleosides. We processed cultures for intracellular and extracellular metabolite extraction as described previously (Fiore et al. 2015; Text S1). For intracellular metabolites, we collected cells via filtration on 0.2 µm PTFE filters (Omnipore, Millipore) and stored them at −80°C. Metabolites were extracted in 500 µl of cold 40:40:20 acetonitrile:methanol:water with 0.1 M formic acid. Extracts were reduced to near dryness under vacuum centrifugation and reconstituted in 500 µl (extracellular) or 643.5 µl (intracellular) of 95:5 MilliQ water:acetonitrile with deuterated biotin (d2-biotin, final concentration 0.05 µg ml^{-1}) added as an HPLC injection standard as per Johnson et al. (2017); a 100 µl aliquot of the extract was used for targeted metabolomics analysis. We extracted extracellular metabolites using solid phase extraction (SPE) with 1 g/6 cc PPL cartridges (BondElut, Agilent) as described elsewhere (Dittmar et al. 2008, Longnecker 2015). During the last time point, 3 cultures in the P-replete treatment required multiple filters to process the culture. For these 3 samples, a known volume of culture was passed through each filter. Two filters per sample were used in metabolite extraction, and the extracts were combined prior to metabolomics analysis.

Intracellular and extracellular extracts were analyzed using targeted metabolomics with HPLC (Thermo PAL autosampler and Accela pump) coupled to tandem mass spectrometry (TSQ Vantage, Thermo Fisher Scientific) via a heated electrospray ionization source operated in both positive and negative ion modes (Kido Soule et al. 2015). All 62 standards were quantified using optimized selected reaction monitoring conditions (XCalibur 2.0) in the intracellular samples (Kido Soule et al. 2015), while 23 metabolites with high SPE recovery (Johnson et al. 2017) were quantified in the extracellular samples. Concentrations of metabolites were calculated based on a 5- to 7-point manually curated external calibration curve (0.5–500 ng ml^{-1}). The calibration curve was water-based, and thus we used pooled samples to assess matrix effects. A pooled sample for quality control consisted of 10 parts intracellular extract and 1 part extracellular extract of each experimental sample and was analyzed every 10 injections (Text S1). A laboratory-fortified pooled sample containing a standard mix was also analyzed at the start, middle, and end of the analytical run to assess matrix effects and analytical quality. Chromatographic peaks derived from calibration standards, pooled samples, and experimental samples were manually assessed for quality, and metabolite concentrations were exported to Excel. The limit of detection (LOD) of each compound in our method was determined using Milli-Q water and was estimated for SPE methods with seawater (Johnson et al. 2017). The LOD ranged

from ~0.4 to 49 ng ml^{-1}, but most were <10 ng ml^{-1} (Johnson et al. 2017). To facilitate comparison with other studies, we also report cell-normalized ratios of the P-deficient to P-replete metabolite concentrations. All metabolomics data are available in MetaboLights (www.ebi.ac.uk/metabolights/) under accession number MTBLS295, and cell- and volume-normalized metabolite concentrations can be found in Dataset S1 in Supplement 2 at www.int-res.com/articles/suppl/a086p029_supp2.xlsx.

While both intracellular and extracellular metabolites were quantified in our experiment, the results and discussion will focus primarily on changes in the intracellular metabolite profile in response to P deficiency, highlighting compounds that were most relevant to the discovery of the *psr*1-like gene. We further focus the intracellular metabolite comparison on the exponential growth phase (T_1) to capture clear changes in metabolite profiles between treatments and facilitate comparison to previous studies (Whitney & Lomas 2016, Bachy et al. 2018). R statistical software (v3.0.2; R Core Team) was used for statistical analyses. We used a Welch's 2-sample *t*-test, followed by Benjamini-Hochberg false discovery rate correction (Benjamini & Hochberg 1995), to compare the cell-normalized concentrations of specific metabolites (log transformed to achieve a normal distribution) between P-deficient and P-replete treatments.

2.3. Identification of the putative phosphate starvation response (*psr*1) gene and putative DNA-binding motifs

We used the *psr*1 gene sequence from *Chlamydomonas reinhardtii* (Wykoff et al. 1999, NCBI XM_001700501.1) to query the genome of *M. pusilla* using the BLAST option through Integrated Microbial Genomes (IMG, blastx, e-value: 1e-5). Conserved domains within putative sequences were characterized using an NCBI conserved domain search (Marchler-Bauer & Bryant 2004). We then used the putative *M. pusilla psr*1-derived amino acid sequence to query several databases using BLAST (tblastn, e-value: 1e-5), including: a re-assembly of the Marine Microbial Eukaryote Transcriptional Sequencing Project (MMETSP) (Johnson et al. 2019), NCBI non-redundant protein sequences (nr), the NCBI metagenome proteins (env nr), the *Tara* Oceans eukaryotic unigenes (Carradec et al. 2018), and several eukaryotic algal genomes from IMG (Text S1). For the *Tara* Oceans data, we selected only the *psr*1-like unigenes from the metatranscriptome assemblies that were assigned the taxonomic classification of *Micromonas*. Within each sample, we normalized the expression of the *psr*1 unigenes to the total abundance of all unigenes taxonomically classified as *Micromonas* (Text S1). Visualization of the *Tara* Oceans queries were performed using the 'basemap' library in Python and custom Python scripts (Text S1). For several genes of interest, we compared the distribution of gene expression to the expression of *Micromonas psr*1-like genes in the *Tara* Oceans metatranscriptome using a Kolmogorov-Smirnov test. We tested a relationship between phosphate concentration and normalized expression of *Micromonas psr*1-like genes from *Tara* Oceans metatranscriptomes by comparing the abundance of *Micromonas psr*1-like transcripts above and below the mean concentration of phosphate using Student's *t*-test.

We manually checked significant matches for all nucleotide sequences that were collected from database-based (NCBI, IMG, MMETSP, *Tara* Oceans) BLAST searches using the *psr*1-like gene from *M. pusilla*. First, we used conserved domain analysis (Marchler-Bauer & Bryant 2004) to assess domain similarity to *psr*1, and second, we used the sequences with both characteristic domains of the *C. reinhardtii psr*1-derived amino acid sequence in a multiple sequence alignment to the *C. reinhardtii psr*1-derived amino acid sequence. Sequences that did not align with the myb coiled-coil domain of *C. reinhardtii* and *M. pusilla* were removed from further consideration. Sequence alignment and phylogenetic analysis was performed in MEGA 7 (Kumar et al. 2016) using MUSCLE (Edgar 2004) with default settings in MEGA. Phylogenetic reconstruction of the *psr*1 gene was performed in MEGA using neighbor-joining, maximum parsimony, and maximum likelihood algorithms and bootstrap replication 500 times. The tree topology for the different phylogenetic reconstructions was similar for nodes with high bootstrap values (>50%, data not shown). We present the maximum likelihood tree because this algorithm (Jones-Taylor-Thornton model, default maximum likelihood settings in MEGA) uses the most information in its alignments and typically has high accuracy (Felsenstein 1981, Kishino et al. 1990). A FASTA file containing the sequences used in the phylogenetic analysis as well as the alignment exported from MEGA (FASTA format) are available online at https://osf.io/92tg4/.

Following the identification of putative *psr*1-like genes in *M. pusilla*, we searched genes of *M. pusilla* CCMP1545 for a regulatory binding element, or motif, where the Psr1-like protein would bind to activate or repress gene transcription. The metabolomic results (see Fig. 1) were used to inform our selection

of genes to be surveyed with the motif analysis. In the survey process, we first searched genes within a now-archived gene model of *M. pusilla* CCMP1545 (FrozenGeneCatalog_20080206 (ver_1), Table S1 in Supplement 1), then we revised our search for binding elements within the updated gene models from Bachy et al. (2018) (*M. pusilla* CCMP1545/MBARI_models(ver_1), Table S1 in Supplement 1). Each *M. pusilla* gene sequence used in the motif analysis consisted of concatenated 500 nucleotides upstream and downstream of the gene as well as untranslated regions and intronic regions, thereby excluding the coding regions. We analyzed gene sequences of interest for a significant conserved motif, using the motif-based sequence analysis tools Multiple Em for Motif Elicitation (MEME Suite) 4.10.1 (Bailey et al. 2009). The genes of interest (Table 1) were selected based on metabolites that were, on average, elevated or depressed in concentration in the P-deficient cultures, although they were not statistically different between treatments (i.e. malate, several amino acids, vitamins, see Fig. 1). These included genes related to central carbon metabolism, lipid metabolism, vitamin metabolism (pantothenate, folate), and nucleotide metabolism (aspartate). We also included genes within the carbohydrate and lipid metabolic pathways based on published work (Hockin et al. 2012, Goncalves et al. 2013) as well as the gene for proline oxidase (POX), a key enzyme up-regulated in *E. huxleyi* in response to N- and P-deficiency (Rokitta et al. 2014, 2016).

After initial motif discovery, we optimized our putative motif by varying motif width and number within genes of interest and within genes that were not expected to be regulated under P deficiency, including asparagine synthetase (Joint Genome Institute [JGI] gene ID: 9681548) and acetyltransferase-like/flavin adenine dinucleotide-linked oxidase [9687568]). We attempted to identify motifs using the motif comparison tool (Tomtom; Gupta et al. 2007) against the *A. thaliana* database (Protein Binding Microarray [PBM] motifs, Franco-Zorrilla et al. 2014), and significant matches were used to guide the optimization of motif discovery settings and inclusive sequences. Using the selected sequences and optimized parameters, we searched for motifs that are overrepresented in the query sequences ('positive') relative to a set of background sequences ('negative'), the latter defined using the genome scaffolds. We used positive and negative sequences to create a position specific prior distribution file (Bailey et al. 2009), for further discriminative motif discovery within *M. pusilla* gene sequences of interest (parameters: minw = 5, maxw = 10, nmotifs = 3, mod = oops [one occurrence per sequence]).

Two recent publications provided transcriptomes for testing our hypotheses regarding expected differentially expressed (DE) genes in P-deficient and P-replete conditions. Whitney & Lomas (2016) published transcriptomes of *M. commoda* (formerly *M. pusilla*) RCC299, while Bachy et al. (2018) published transcriptomes of *M. pusilla* CCMP1545, under P-deficient or P-limiting (respectively) and P-replete conditions. Genes discussed here as DE were defined by each study (Whitney & Lomas 2016, Bachy et al. 2018). We first compared our hypothesis for genes that would be differentially regulated in *M. pusilla* to observations in Bachy et al. (2018). We also used the information from Bachy et al. (2018) to inform our targeted search for a significant conserved motif in genes that may be regulated by the Psr1-like TF. We note that each *Micromonas* experiment used slightly different growth conditions and were sampled at different stages of growth. Thus, we focus our comparisons on work in the same strain (*M. pusilla* CCMP1545, Bachy et al. 2018), with brief complementary discussions about *M. commoda* (expanded results in Text S2 in Supplement 1). Bachy et al. (2018) used semi-continuous cultures grown under continuous light and with a moderately higher concentration of P (2.5 µM) than in our experiment (0.4 µM). Despite these differences, the transcriptional data of *M. pusilla* under P limitation provided a preliminary test of our hypotheses derived from the metabolomics analyses with *M. pusilla* CCMP1545 and *in silico* genomic analysis. We further reasoned that a signal observed across species and experiments would likely represent a conserved and biologically meaningful response to P deficiency.

3. RESULTS

3.1. Metabolic response of *Micromonas pusilla* CCMP1545 to P deficiency

Quality control analysis of the d2-biotin injection standard described above indicated low ionization variability across the pooled samples (coefficient of variation [CV] = 8.5%) and the intracellular samples (CV = 20%), but higher variability across extracellular samples (CV = 65%). This is likely a result of the dissolved organic carbon background from seawater in the extracellular extracts (but absent in the intracellular) coeluting with d2-biotin, causing matrix interference. Previous work using spent media from *M. pusilla* observed no significant matrix effect on the instrument response factor for most of the metabolites assessed by the same targeted metabolomics

Table 1. Enzymes that contain a significant motif in the gene sequences of *Micromonas pusilla* CCMP1545 (MBARI_models (ver 1)) and contain a putative myb-like DNA-binding domain. EC number: Enzyme Commission number or pfam identifier; pathway: main pathway(s) in which the enzyme is involved. Fold change and *q*-values of the transcript in P-deficient relative to P-replete conditions are data from Bachy et al. (2018) and are given with the corresponding Joint Genome Institute (JGI) gene ID. CoA: coenzyme A; TCA: tricarboxylic acid; ETC: electron transport chain

Enzyme	EC number	Pathway	Log2 fold change	*q*-value	JGI gene ID
Glyceraldehyde-3-phosphate dehydrogenase	1.2.1.12	Calvin cycle/glycolysis	2.73	0.000037	4267
Glyceraldehyde-3-phosphate dehydrogenase	1.2.1.12	Calvin cycle/glycolysis	−0.644	0.000037	700
Phosphoglycerate kinase	2.7.2.3	Glycolysis	−0.699	0.000037	7661
Pyruvate kinase	2.7.1.40	Glycolysis	−1.32	0.000037	9370
Pyruvate dehydrogenase	1.2.4.1	TCA cycle/glycolysis	0.756	0.000037	3535
Citrate synthase	2.3.3.1	TCA cycle	1.68	0.000037	1278
Citrate synthase	2.3.3.1	TCA cycle	1.10	0.000037	3714
Aconitase	4.2.1.3	TCA cycle	1.00	0.000037	2901
Succinate dehydrogenase	1.3.5.1	TCA cycle and ETC	1.16	0.001515	2182
Fumarase	4.2.1.2	TCA cycle	1.68	0.000037	600
Fumarase	4.2.1.2	TCA cycle	1.73	0.000068	6662
Copper amine oxidase	1.4.3.21-22	Arginine and proline metabolism	2.87	0.000037	5863
Aspartate transcarbamylase	2.1.3.2	Pyrimidine biosynthesis	−0.609	0.000037	3615
Nucleoside phosphatase	3.6.1.3	Pyrimidine metabolism	0.711	0.000037	3322
Pantoate-beta-alanine ligase	6.3.2.1	Pantothenate and CoA biosynthesis	−0.616	0.000037	5304
Lysophospholipase	3.1.1.5	Glycerophospholipid metabolism	1.65	0.000037	3652
Acyl-CoA synthetase	6.2.1.3	Fatty acid metabolism	3.20	0.000037	1751
Long-chain acyl-CoA synthetases	6.2.1.3	Fatty acid metabolism	0.736	0.000037	416
Na+/PO_4 transporter	PF02690	Inorganic nutrient transport	4.54	0.000037	5963

method that we used here (Johnson et al. 2017). In this experiment, we quantified 21 metabolites from that study (Fig. S2 in Supplement 1) and of these, 8 were shown to exhibit ionization suppression in the *M. pusilla* extracellular extracts (Johnson et al. 2017). Thus, we have used caution in the interpretation of the extracellular metabolite comparisons between treatments (Fig. S2).

Metabolite concentrations in the extracellular fraction (Fig. S2) were generally lower under P deficiency relative to the P-replete cultures, although these differences were not statistically significant between treatments (*t*-test, $p > 0.05$). The extracellular metabolite concentrations were standardized to the number of cells in each sample and represent cumulative changes in the media over time. We note that some core metabolites may be present below the limit of detection of our method (Johnson et al. 2017).

In contrast, there was a mixed response in metabolite concentrations in the intracellular fraction. Several of the intracellular metabolites, standardized to cell number, were abundant under P deficiency during exponential growth (T_1), including nucleobases (xanthine, adenine), the nucleoside inosine, amino acids (glutamine, aspartate), the amino acid derivatives *N*-acetylglutamate and tryptamine, the dicarboxylic acid malate, and vitamins (thiamin, pantothenate, folate) (Fig. 1). Due to high variability in our treatments, we did not observe statistically significant results after p-value correction (*t*-test, $p > 0.05$). However, we observed decreases in the intracellular ratios of purine nucleosides (guanosine, xanthosine) to their nucleobases (guanine, xanthine) under P deficiency at T_1 (Fig. 2). The decrease in the xanthosine:xanthine ratio was statistically significant (*t*-test, $p = 0.03$). The change in the guanosine:guanine ratio could not be statistically tested, as guanine was below detection in 2 of 3 P-replete cultures (Fig. 2). The di- and tricarboxylic acids malate, succinate, and citrate exhibited divergent responses, although their abundances were not significantly different between treatments (Fig. 1). Malate was more abundant in P-deficient cells, while succinate concentrations were similar between treatments and replicates; citrate was detected in only 1 of 3 replicates in each treatment (Fig. 1). We noted similarly varied responses to P deficiency in the purine nucleosides xanthosine and inosine, with invariant xanthosine abundances but higher average concentrations and variability of inosine (Figs. 1 & 2).

3.2. Characterization of the phosphate starvation response (*psr*1) gene in marine algae

We found 4 statistically significant sequences (Table 2) in response to querying the now-archived *M. pusilla* CCMP1545 genome with the *psr*1 gene from *Chlamydomonas reinhardtii* (strain cc125, NCBI accession AF174532). One of these sequences (JGI ID 61323) had the 2 characteristic myb domains of the *psr*1 gene in *C. reinhardtii* (myb-like DNA-binding domain, SHAQKYF class [TIGR01557] and myb predicted coiled-coil type transfactor, LHEQLE motif [pfam PF14379]) (Fig. 3A). However, the helix-turn-helix dimerization domain and glutamine-rich regions that are characteristic of TF activation domains, as well as the putative metal-binding domain originally described for *psr*1 in *C. reinhardtii* (Wykoff et al. 1999) were not detected in the putative *M. pusilla psr*1 gene. Thus, we refer to the gene in *M. pusilla* as a *psr*1-like gene (Fig. 3; Fig. S3 in Supplement 1). Conserved domain analysis (Marchler-Bauer & Bryant 2004) revealed 2 other domains in the putative *psr*1-like-derived amino acid sequence from *M. pusilla*: (1) PLN03162 super family (NCBI cl26028), a provisional golden-2 like TF, and (2) a DUF390 super family domain (NCBI cl25642), comprising proteins of unknown function (Fig. S3). A comparison of homology of the *psr*1-like gene between *M. pusilla*, *M. commoda*, *C. reinhardtii*, and *Arabidopsis thaliana* is provided in Table S2 in Supplement 1.

We identified putative *psr*1-like genes or transcripts in cultured isolates as well as in field datasets (see Figs. 3b, 4, & 5; Table S3 in Supplement 1),

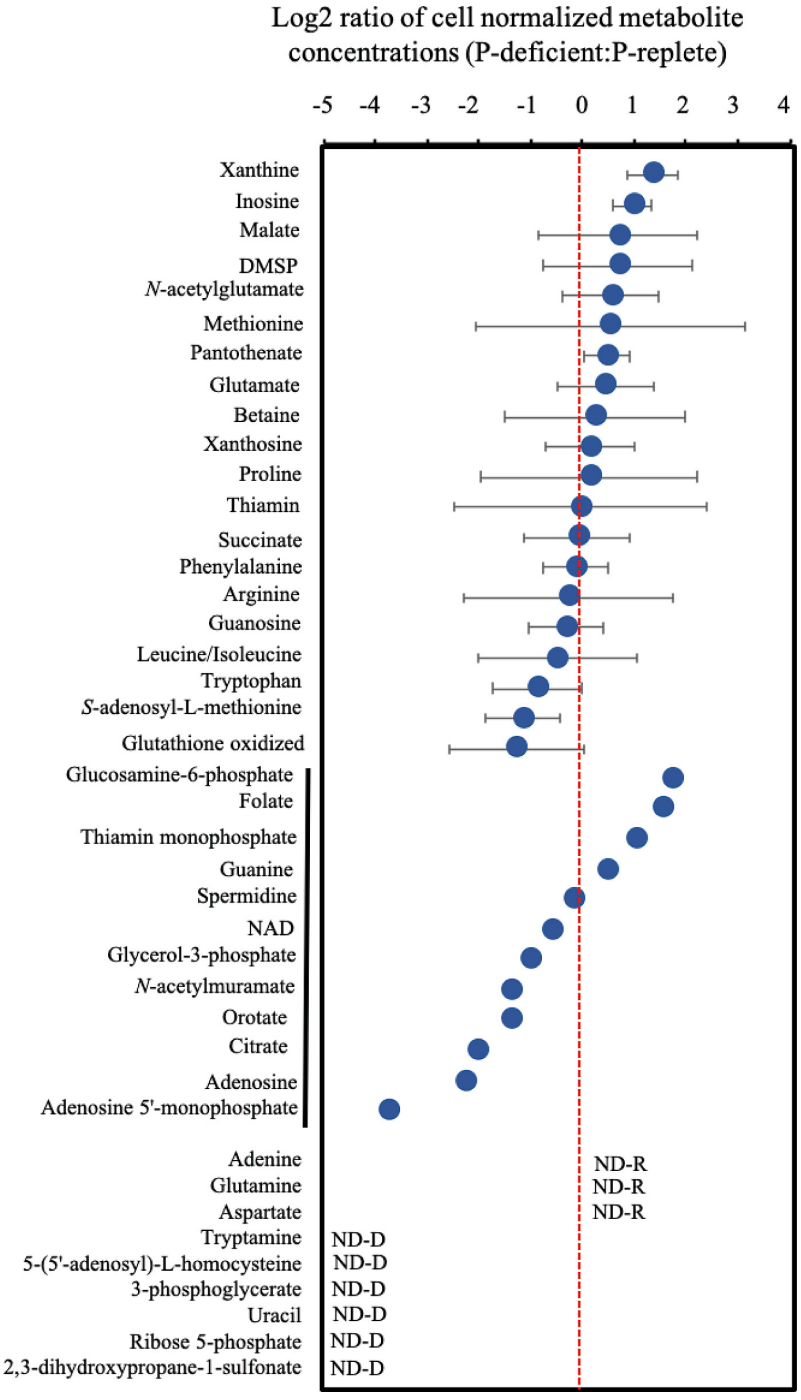

Fig. 1. Log2 of the average ratio of the P-deficient to P-replete intracellular metabolite concentrations during exponential growth (T_1) in *Micromonas pusilla* CCMP1545. Concentrations were normalized to cell number in each treatment and means (± propagated uncertainty) are shown (N = 3 unless otherwise noted). Red dashed line indicates a ratio of 0, where the concentrations of the metabolites are the same between treatments. Metabolites are listed in order of descending value of the ratio within 3 groups: those that were detected in enough replicates for uncertainty to be calculated, those where only 1 ratio could be calculated (black line), and those that were not detected (ND) in any of the 3 replicates for one treatment (R = P replete, D = P deficient). Only 1 replicate in the P-deficient treatment contained a non-0 concentration for *N*-acetylmuramic acid; thus, while there was a significant difference in concentration for this metabolite, only 1 ratio could be calculated. DMSP: dimethylsulfoniopropionate; NAD: nicotinamide adenine dinucleotide

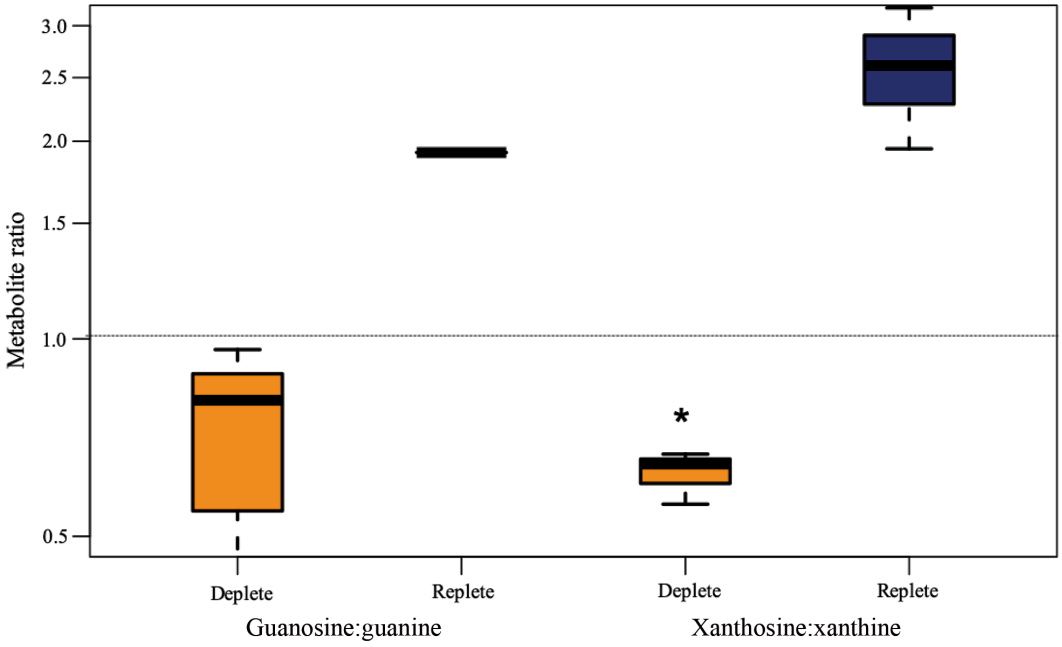

Fig. 2. Intracellular ratios of 2 purine nucleosides to their nucleobases for *Micromonas pusilla* CCMP1545 in P-deficient and P-replete treatments during exponential growth (T_1). The box extends from the first quartile to the third quartile with a thick line at the median, and the whiskers represent the minimum and maximum values. Xanthosine and xanthine, and guanosine and guanine were quantified in the targeted metabolomics method and normalized to cell abundance. The average ratio and high and low values are shown based on 3 replicate cultures. The asterisk marks a significant difference between the treatments (*t*-test, p = 0.03). The dashed line represents a metabolite ratio between treatments of 1. Two samples in the P-replete treatment had guanine levels below the limit of detection and the one ratio is shown as a line

Table 2. Gene matches to *psr*1 in *Micromonas pusilla* CCMP1545 as originally discovered in the Joint Genome Institute (JGI) Integrated Microbial Genomes (IMG) database and the corresponding gene in the updated gene model for CCMP1545 (MBARI_models (ver 1)). The *M. pusilla* CCMP 1545 database in IMG contained 10660 sequences and 4795637 letters. The top-scoring gene was considered to be a *psr*1-like gene and the JGI gene ID is shown in parentheses. The corresponding *psr*1-like gene in the updated gene model is shown for reference, and includes the JGI gene ID, the gene description, and the E-value from the BLAST search (see Section 2) using the top scoring gene (61323) from CCMP1545

IMG gene ID	Locus tag	Bit score	E-value
2615011133 (JGI 61323)	MicpuC2.est_orfs.1_306_4269596:1	90.5	2×10^{-19}
2615008475	MicpuC2.EuGene.0000130210	74.3	4×10^{-14}
2615010887	MicpuC2.est_orfs.10_1861_4270447:1	70.5	3×10^{-13}
2615007841	MicpuC2.EuGene.0000090108	67.8	4×10^{-12}
JGI ID 360	Myb domain-containing protein		8×10^{-156}

representing diverse taxa such as Dinophyta (e.g. the symbiotic clade C *Symbiodinium* sp.) and Haptophyta (e.g. the coccolithophore *Emiliania huxleyi*). In our phylogenetic analysis (Fig. 4), sequences generally clustered by taxonomic group with multiple clades of Chlorophyta across the tree (Fig. 4). However, the clades with other groups such as haptophytes (e.g. *Chrysochromulina rotalis* and *E. huxleyi*) are not well resolved (Fig. 4; Fig. S4 in Supplement 1). There were also relatively few non Chlorophyta-derived sequences that could be included in the alignment due to low quality (i.e. short sequence length).

Transcripts from MMETSP and *Tara* Oceans, as well as high-identity hits to sequences from the Global Ocean Sampling expedition (GOS, Rusch et al. 2007), were generally short sequences and often contained 1 of the 2 characteristic domains for *psr*1-derived amino acid sequences (Text S2). Field-derived transcripts of the *psr*1-like gene were geographically dispersed in the *Tara* Oceans dataset with the highest relative expression in surface samples and in the North Atlantic Ocean and Mediterranean Sea (Fig. 5A). The majority of these transcripts from the *Tara* Oceans dataset occurred in samples with low phosphate concentrations (≤0.5 µM), but there was no significant relationship between *psr*1-like gene expression and phosphate concentration (*t*-test, $p < 0.05$;

A)

Micromonas pusilla CCMP1545: 2615011133

MTRMSGIEDDSFSYSFLLISGQLRDPTRLTPRPQTSSAPLGAGGGAAAASGMNTSGTFWPSDLDLDLESSDFL
DSLLLGGEMMTTQQQHHHAGDERLGHGPVPLGARAAGEDHDPRVVLAERDAGDGLLPRALADERREPVAR
AVVASNNNKQRLRWTPELHKMFVDAVKRLGGLDLATPKGIMQLMDVEGMSIQHVKSHLQKYRLQDSGGG
ASEFRVSPDASASGKRPRSEEDDAGGNGKDGNNSAGKTRRRPSAAERSAARLRAAEEKAREERDAARSMAA
AAAAAAAAAVERQNVELALLTGDAAGARDALEMSSHHAASHVGGAYDDVLDLVAGPGESGDGDGAWGD
VLHDHAIVGAAGDDVGLVDDVGSDPEAAAAMLKQLELQKKLHEHLMSQRRLQQQVEAHGVYLETILDQQK
RRRGVE

B)

	S H L Q K y R		L H E Q L
	* * * * * * *		
Arabidopsis thaliana NC_003075.7	P K G V L K I M K V E - G - - - L T I Y H V K S H L Q K Y R	278	L H - E Q L 331
Volvox carteri XP_003054945.1	P K G I L K L M C L E - G - - - L T I Y H I K S H L Q K Y R	326	L H - E Q L 457
Micromonas pusilla CCMP 1545 2615011133 (IMG)	P K G I M Q L M D V E - G - - - M S I Q H V K S H L Q K Y R	205	L H - E H L 396
Ostreococcus lucimarinus 640420317 (IMG)	P K G I M H I M A M S - G - - - M T I Q H I K S H L Q K Y R	170	L H - D Q L 320
Micromonas sp. RCC 299 XP_002504000.1	P K G I M Q L M E V D - G - - - M T I Q H V K S H L Q K Y R	240	L H - A Q L 416
O. tauri 2507574032 (IMG)	P K G I A T L M T T S - G - - - M T L Q H I K S H L Q K Y R	106	L H - D Q L 241
GOS marine metagenome EBR92606.1	P K R I L D L M G V Q - G - - - L T R E N V A S H L Q K Y R	54	P D G G M M 201 *
GOS marine metagenome EBU22100.1	P K G I M H I M A M S - G - - - M T I Q H I K S H L Q K Y R	67	- - - - - - - 84 *
GOS marine metagenome EBY01923.1	P K G I M S L M T T A - G - - - M T L Q H I K S H L Q K Y R	133	L H S M D A 223 *
Emiliania huxleyi XP_005765367.1	P Q A I S Q L M N C E - G E G A P T R Q N I K S H L Q K Y R	161	L E - - - - 212 *
GOS marine metagenome EDD34186.1	P Q A I R Q L M G C K T E E E A P T R Q N I K S H L Q K Y R	228	L H - E Q Q 327 *
Chlamydomonas reinhardtii NW_001843857.1	P K G I L K L M G V D - G - - - L T I Y H I K S H L Q K Y R	240	L H - E Q L 403
Chlorella variabilis 2507982799 (IMG)	P K R I L D L M N V E - G - - - L T R E N V A S H L Q K Y R	253	- - - - - - 334 *
MMETSP0052 *Polymella parva*	P K G I V T L M N V R - E - - - I T I Y H V K S H L Q K Y R	239	T A N A T L 425 *
MMETSP0063 *Chlamydomonas euryale*	P K K I L E I M Q V E - D - - - L T R E N I A S H L Q K Y R	293	G G - - - - 361 *
MMETSP1127 *Dunaliella tertiolecta*	P K G I L K L V N S E - G - - - L T I Y H I K S H L Q K Y R	247	F Q G A G G 335 *
MMETSP1460 *Bathycoccus prasinos*	P K G V V E L M R V Q - G - - - V T I P H V K S H L Q K Y R	192	L H - E Q L 452
MMETSP1106 *Mantoniella antarctica*	P K G I M Q L M G V T - G - - - M T I Q H V K S H L Q K Y R	237	S A - A R I 332 *
MMETSP1403 *M. pusilla* CCMP 1723	P K G I M Q L M E V E - G - - - M T I Q H V K S H L Q K Y R	238	L H - E Q L 413
MMETSP0384 *Alexandrium tamarense*	P K T I L Q L M N V E - G - - - M T R E N V A S H L Q K Y R	97	M G - - - - 176 *
MMETSP1369 *Symbiodinium* sp. C1	P K N I M Q E M N V E - G - - - L T R E N V A S H L Q K Y R	113	- - - - - - 110 *
TARA MATOU-v1_62935935	P K G I M H I M A M S - G - - - M T I Q H I K S H L Q K Y R	57	- - - - - - 74 *
TARA MATOU-v1_45631074	P K G V V E L M R V Q - G - - - V T I P H V K S H L Q K Y R	88	L H - E Q L 348
TARA MATOU-v1_79753402	P K L I L R L L A V P - G - - - M T I Y H V K S H L Q K Y R	146	L Q - E Q L 243
TARA MATOU-v1_83305352	P K F I M R L L A V P - G - - - M T I Y H V K S H L Q K F R	87	L R - E Q L 158 *

Fig. 3. Predicted amino acid sequences of the *psr*1-like gene in *Micromonas pusilla* CCMP1545 and a subset of other organisms. The amino acid sequence (with IMG gene ID) is shown as described in the Joint Genome Institute Integrated Microbial Genomes *M. pusilla* CCMP1545 database. (A) The myb-like DNA-binding and myb coiled-coil domains are highlighted in blue. (B) Predicted amino acid sequence alignment of *psr*1 and *psr*1-like genes in the region of the myb-like DNA-binding domain (SHAQKYF class) and LHEQL coiled-coil domain. Note that not all sequences contain the LHEQL domain as characterized by CD-Search (Marchler-Bauer & Bryant 2004); these are marked with an asterisk on the right side of the alignment. Asterisks at the top of each column indicate 100% conserved residues across species surveyed. Numbers at the end of each row indicate position of the last shown residue in the amino acid sequence. Accession (GOS, MMETSP, NCBI, *Tara*) or gene identification (IMG) numbers are listed for each sequence

Fig. 5B). We observed a significant positive relationship (Kolmogorov-Smirnov, $p < 0.05$) between the presence of *Micromonas psr*1-like genes and the relative expression of fumarase, a tricarboxylic acid (TCA) cycle gene in *Micromonas*, which was up-regulated in cultures of *M. pusilla* (Bachy et al. 2018) and *M. commoda* (Whitney & Lomas 2016) under P deficiency (Fig. 5C; Text S3 in Supplement 1). We did not find genes with significant homology to the *M. pusilla* putative *psr*1-like gene, in genomes or transcriptomes, within diatoms, the Heterokonta superphylum, or the cryptophytes.

3.3. Putative regulatory element in *M. pusilla* genes of interest

MEME analysis yielded a significant conserved motif in *M. pusilla* genes involved in central carbon metabolism, lipid metabolism, and nucleotide metabolism (Fig. S5 in Supplement 1). The genes of interest for MEME analysis (Table 1) were selected based on our metabolomics results and informed by the literature (see Section 2.3). The significant conserved motif is similar in nucleotide sequence to several TF-binding sites in *A. thaliana* (Table S4 and Fig. S6 in

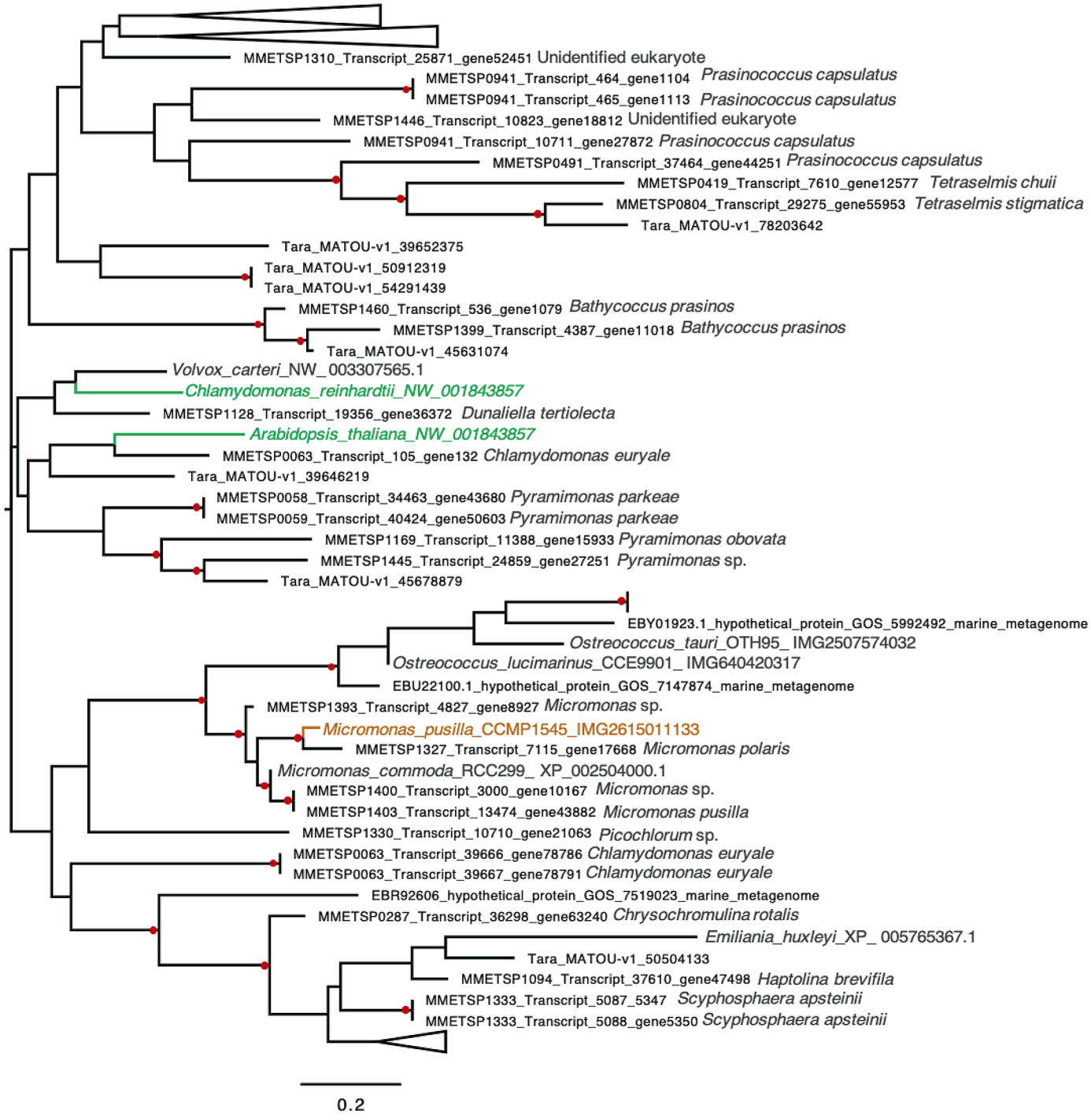

Fig. 4. Occurrence and phylogenetic relationship of *psr*1-like genes in marine phytoplankton. All sequences that included the conserved SHLQKYR and LHEQL domains (see Fig. 3) were included in the alignment (see Section 2 for details), with the exception of 2 global ocean survey (GOS) sequences and the *Emiliania huxleyi* sequence. These sequences were short sequences and only contained the SHLQKYR domain, but were included for context. Several branches are collapsed for clarity and the full tree is shown in Fig. S4. Maximum likelihood method is based on the JTT matrix-based model (Jones et al. 1992). The tree with the highest log likelihood (–4344.61) is shown and is based on the derived amino acid sequences for *psr*1 and *psr*1-like genes from eukaryotic phytoplankton. Bootstrap support for branches that are ≥50% are marked with a red circle. The tree is unrooted and drawn to scale, with branch lengths measured in number of substitutions per site. The analysis involved 80 amino acid sequences. All positions containing gaps and missing data were eliminated. The final dataset included a total of 66 positions. Evolutionary analyses were conducted in MEGA7 (Kumar et al. 2016). *Micromonas pusilla* CCMP1545 used in this study is colored brown, and genes that have been functionally characterized are colored green (Rubio et al. 2001, Moseley et al. 2006, Bajhaiya et al. 2017).

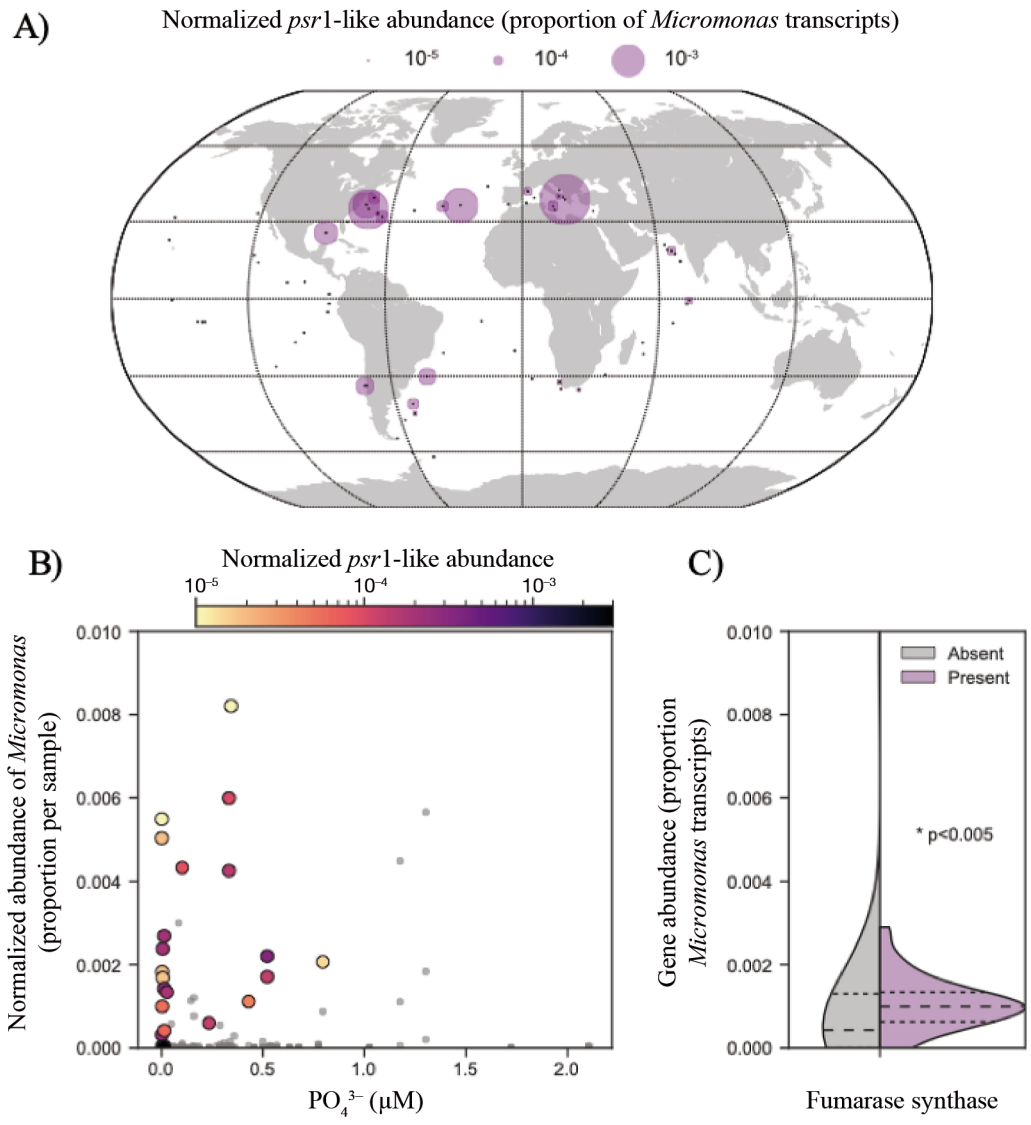

Fig. 5. Geographic distribution of *Micromonas psr*1-like genes and relationship with phosphate concentration in the *Tara* Oceans eukaryotic gene atlas (Carradec et al. 2018). (A) Geographic distribution and relative abundance of *Micromonas psr*1-like genes in surface samples. Black dots represent stations where *Micromonas* was detected; the size of purple circles represents the relative abundance of the *psr*1-like gene, where the fragments per kilobase million (FPKM) of the *psr*1-like gene was normalized to the total FPKM of all *Micromonas*-associated transcripts. (B) Relative abundance of *Micromonas* plotted against phosphate concentrations for surface stations where *Micromonas* was detected. Grey circles indicate samples where *psr*1-like genes were not detected, while samples where *psr*1-like genes were detected are colored based on the relative expression of the *Micromonas psr*1-like gene, again normalized to total *Micromonas* transcript abundance. No significant relationship was observed between the phosphate concentration and abundance of *Micromonas psr*1-like transcripts (*t*-test, $p > 0.05$). (C) Distribution of the expression of *Micromonas* fumarase synthase genes as a function of presence or absence of the *psr*1-like gene. The larger dashed line represents the distribution mean and the smaller dashed lines represent the 25 and 75% quartiles. Significant difference in the distribution of expression between the presence and absence was assessed with a Kolmogorov-Smirnov test ($p < 0.005$)

Supplement 1, Franco-Zorrilla et al. 2014), including myb-like TF-binding motifs. The presence of a myb-like TF-binding motif is notable as the Psr1 protein contains a myb-like DNA-binding domain (Wykoff et al. 1999). Several iterations of this analysis using genes not tied to the metabolites of interest yielded either no significant motif or motif sequences lacking similarity to myb-like domains. We observed a similar significant conserved motif in author-defined DE transcripts (Bachy et al. 2018) in *M. pusilla* CCMP1545 under P deficiency (Table 1; Fig. S5). While the actual nucleotide sequence recognized by a TF must be experimentally determined (Franco-Zorrilla et al. 2014), the presence of a significant

conserved motif in each model, and only in the expected genes, indicates that this motif is likely biologically significant in *M. pusilla*. Specifically, this motif, with similarity to myb-like domains in *A. thaliana*, may represent a regulatory element where the Psr1-like protein binds.

3.4. Comparison of metabolomics-based predictions of P-responsive genes in *M. pusilla* CCMP1545 to transcriptomics analysis

We compared the author-defined DE transcripts in *M. pusilla* CCMP1545 to gene predictions based on our metabolomics data. As Bachy et al. (2018) used a more recent gene model than our original analysis, we confirmed the identity of the *psr*1-like gene in the updated model (CCMP1545/MBARI_models(ver_1), Table 2). We then analyzed a similar set of genes for a regulatory element where the Psr1-like TF might bind (Fig. S5), including genes that were DE in the P-deficient transcriptome relative to the replete transcriptome (Table S1 from Bachy et al. 2018). Under P deficiency, the *psr*1-like gene (JGI gene ID 360) was highly up-regulated (log-2 fold-change = 4.3, q = 0.00037), and nearly all of the predicted P-responsive genes were DE (Table 1). For example, *M. pusilla* up-regulated many genes in the TCA cycle but not pyruvate carboxylase (gene ID 6984). Genes involved in nucleotide and lipid metabolism (e.g. nucleoside phosphatase, long-chain acyl-coA synthetase) were DE and contained a significant conserved motif with similarity to the myb-like regulatory element in *A. thaliana* (Table 1, Fig. S5). Lastly, the POX-encoding gene described in *E. huxleyi* (Rokitta et al. 2016) and observed in the archived gene model for *M. pusilla*, was absent, or not similarly annotated in the updated gene model. Instead, a copper amine oxidase (gene ID 5863) contained a significant conserved motif (Table 1, Fig. S5) and was DE under P deficiency (Bachy et al. 2018).

We conducted a similar analysis with published transcriptome data from *M. commoda* (Whitney & Lomas 2016). The *psr*1-like gene (JGI gene ID 60184) in *M. commoda* was significantly up-regulated in the P-deficient treatment (defined by Whitney & Lomas 2016; Table S5 in Supplement 1), and we found a significant conserved motif in 18 DE genes. The significant conserved motif identified in *M. commoda* differed in sequence from that discovered in *M. pusilla* and occurred in a different set of genes (Text S2).

4. DISCUSSION

Our combined metabolomics and comparative genomic analyses of the response of *Micromonas pusilla* CCMP1545 to P deficiency has led to 3 conclusions: (1) there was an observable shift in intracellular metabolite composition, (2) a *psr*1-like gene is expressed in *M. pusilla* and other marine phytoplankton, and (3) the genes regulated by the Psr1-like protein may differ amongst algal species.

4.1. *M. pusilla* exhibits a metabolic shift in response to P deficiency

In the extracellular media, some metabolites such as guanosine, pantothenate, 2,3-dihydroxybenzoate, and leucine, and inosine were lower in concentration on average in the extracellular P-deficient treatment, but there were no significant differences between treatments. A reduction in many metabolites involved in central metabolism would be expected, as nutrient-limited microalgae may have lower photosynthetic activity (Loebl et al. 2010, Halsey et al. 2014, Guo et al. 2018) and hence produce less metabolic overflow. The high variability across replicate cultures is likely a factor in the lack of significance in concentration between treatments, and there may be other metabolites not quantified here that are significantly different in concentration between treatments. The lack of significant differences in the quantified extracellular metabolites could also indicate regulation of cellular metabolism that impacts metabolic overflow.

The intracellular metabolites did not differ in concentration between treatments; however, we found examples of functionally related metabolites that behaved differently. For example, in the TCA cycle, malate was variable but higher in concentration on average under P deficiency, while citrate was lower on average and succinate was relatively unchanged. The opposing responses of these TCA intermediates was notable given that others (e.g. Hockin et al. 2012, Goncalves et al. 2013, Alipanah et al. 2018) have observed a coordinated response to nutrient limitation in transcripts or proteins involved in the TCA cycle. Specifically, the diatom *Phaeodactylum tricornutum* was observed to down-regulate genes involved in the TCA cycle with simultaneously low concentrations of TCA cycle intermediates under P deficiency (Alipanah et al. 2018). We also observed additional non-uniform metabolite responses, with concentrations of some vitamins (e.g. pantothenate) and amino acids and derivatives (e.g. malate, *N*-

acetylglutamate) higher on average under P deficiency, while other vitamins and organic acids (e.g. thiamin, *N*-acetylmuramate) were depleted or more variable across treatments (Fig. 1). Metabolites that contain P, such as adenosine 5′-monophosphate, glycerol-3-phosphate, and 3-phosphoglycerate were generally depleted and variable in concentration in the P-deficient treatment (Fig. 1).

Previous work has suggested that organisms placed under nutrient stress are capable of diverting carbon flux between pathways (reviewed by Markou & Nerantzis 2013). While metabolite concentrations are regulated at multiple levels, including post-transcriptional modification and enzymatic regulation, another means is through transcription of enzyme-encoding genes. If the shunting of carbon is a coordinated response to P deficiency within *M. pusilla*, then it is possible that genes involved in the synthesis and/or catabolism of these metabolites are co-regulated, and potentially mediated by a specific TF. Motivated by the description of a phosphate starvation response gene (*psr*1) containing a myb DNA-binding domain by Wykoff et al. (1999), and by the non-uniform metabolite patterns that we observed, we investigated the presence of a *psr*1 gene and a myb-like motif in genes that could be regulated by the *psr*1 gene product in *M. pusilla*. Indeed, we discovered a gene in *M. pusilla* and other marine algae with significant homology to the TF phosphorus starvation response gene (*psr*1) originally described in the freshwater alga *Chlamydomonas reinhardtii* (Wykoff et al. 1999).

4.2. Presence and expression of the TF gene *psr*1 in marine algae

In *C. reinhardtii* and in many plants, a *psr*1 gene encodes for a TF (Psr1) that coordinates the metabolic response to P deficiency in these organisms (Wykoff et al. 1999, Moseley et al. 2006, Bajhaiya et al. 2017). We detected a putative *psr*1-like gene in the *M. pusilla* genome, as well as in the genomes and transcriptomes of major algal lineages (e.g. prasinophytes, dinoflagellates). The *psr*1-like genes that we discovered were generally not annotated as *psr*1, with the exception of *Ostreococcus tauri* (Derelle et al. 2006). To our knowledge, however, the potential role of this gene in the metabolism of *O. tauri* or other marine algae has not been discussed. No *psr*1-like gene was identified by our queries of diatom transcriptomes or genomes, suggesting that a phosphate starvation response gene akin to *psr*1 is present in diverse but phylogenetically constrained phytoplankton groups.

We found significant similarity between the *M. pusilla psr*1-like gene and transcript sequences from the MMETSP and *Tara* Oceans metatranscriptomic datasets, indicating that this gene is expressed by marine algae in both cultures and in the environment. High-identity hits to sequences in the metagenomic dataset from the GOS (Rusch et al. 2007) and the *Tara* Oceans metatranscriptomes underscore the prevalence of this gene in the oceans, particularly in regions characterized by chronically low P concentrations. Short sequences in some MMETSP, GOS, and *Tara* Oceans sequences did not include enough of the C-terminal end to capture the myb coiled-coil domain. Thus, further investigation is required to confirm whether the identified transcripts are from *psr*1-like genes. Several GOS sequences, previously described as protein of unknown function, had homology to one of the characteristic Psr1 domains. It is possible that with further characterization, they could be re-annotated as *psr*1-like genes. The prevalence of *psr*1-like genes in the field datasets in particular highlights the need to elucidate the role of a *psr*1-like gene in these organisms.

4.3. Potential role of Psr1 in the marine algal response to P deficiency

TFs typically recognize a specific motif in DNA where the protein binds to regulate each gene. If such a motif is observed, one can hypothesize that a gene containing the motif is regulated by the protein. We observed a conserved and enriched motif across genes involved in nucleotide biosynthesis, the TCA cycle and glycolysis, carbon fixation, fatty acid metabolism, and phosphate transport or salvage (Fig. 6). The significant conserved motifs discovered in both *M. pusilla* and *M. commoda* had unique sequences and were present in a slightly different set of genes (Text S3). The motif detected in *M. pusilla* is similar in nucleotide sequence to a myb regulatory element in *Arabidopsis thaliana.* This similarity is potentially significant, because the *psr*1/*phr*1 genes in *C. reinhardtii* and *A. thaliana* contain a myb DNA-binding domain. Thus, we hypothesize that the significant conserved motif detected in the *Micromonas* species represents binding sites for the Psr1-like TFs.

We observed the significant conserved motif in both *Micromonas* species only in DE genes under P deficiency (Whitney & Lomas 2016, Bachy et al. 2018), suggesting that these genes could be co-regulated. In bacteria, for example, genes within the well-characterized phosphate (Pho) regulon all contain

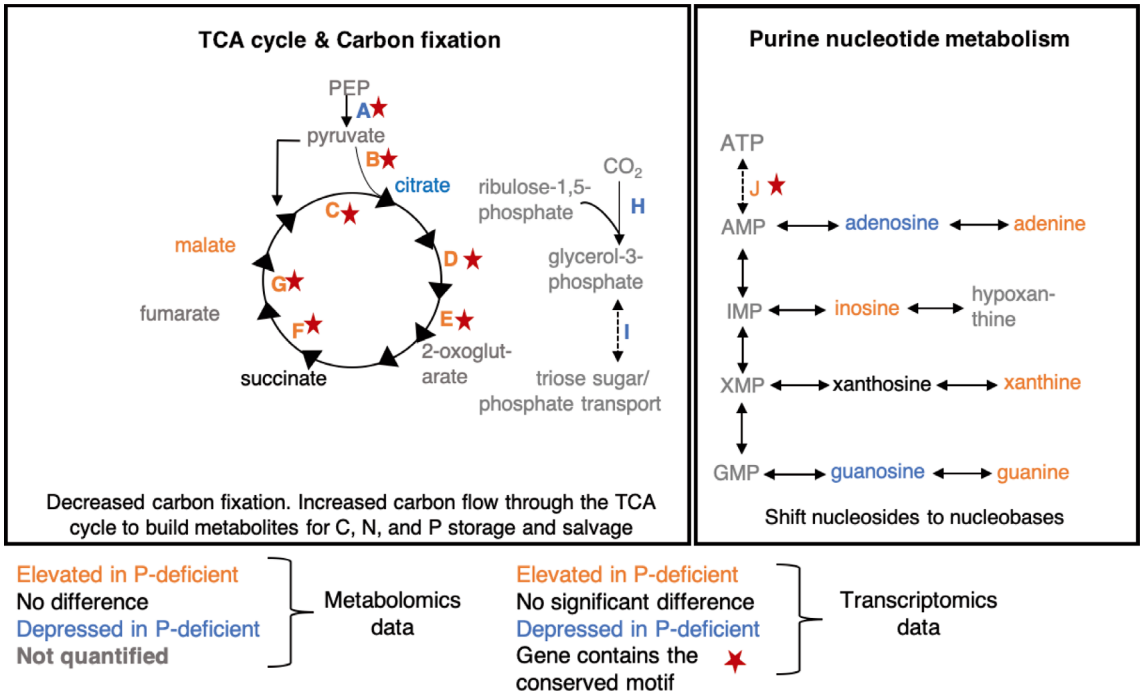

Fig. 6. Conceptual model of Psr1-like transcription factor regulation in *Micromonas pusilla* CCMP154 in 2 major metabolic pathways under phosphorus deficiency. The figure illustrates the relevant metabolites quantified in the present study and indicates if they are elevated (orange, ratio > 0; Fig. 1) or depressed (blue, ratio < 0; Fig. 1) in concentration in the P-deficient cells relative to the P-replete cells. Some metabolite concentrations were equal in each treatment (black) or were not quantified (gray). Genes that contain the conserved motif with similarity to the myb-like regulatory element in *Arabidopsis thaliana* are marked with a red star. The orange and blue letters refer to elevated or depressed transcript levels for each gene (data from Bachy et al. 2018). Descriptions of putative metabolic responses in each pathway are shown. Genes encode for: (A) pyruvate kinase, (B) pyruvate dehydrogenase, (C) citrate synthase, (D) aconitase, (E) α-ketoglutarate dehydrogenase, (F) succinate dehydrogenase, (G) fumarase, (H) ribulose-1,5-bisphosphate carboxylase, (I) triose sugar transporter, (J) nucleotide phosphatase. TCA: tricarboxylic acid

specific sequences (the PHO box) where the TF binds to activate or repress the gene (Santos-Beneit 2015). These PHO box sequences are distinct among different bacterial species and strains. In *M. commoda*, the discovered motif was not significantly similar to myb-like DNA-binding motifs in *A. thaliana* nor was it similar to the motif discovered in *M. pusilla*. Although we expected that the myb domain of the Psr1-like proteins in the 2 *Micromonas* species would interact with similar binding regions in the genome, *psr*1-like derived amino acid sequences from *M. pusilla* and *M. commoda* were only 47% similar. TF protein sequences with up to 79% similarity have been shown to have distinct DNA-binding motif profiles (Franco-Zorrilla et al. 2014), so the 2 proteins in different species could reasonably have distinct DNA-binding motifs. If the Psr1-like TF regulates a different set of genes in the 2 *Micromonas* species, this may serve as a niche-defining feature between these taxa similar to that described in yeast (Borneman et al. 2007). As further support for this hypothesis, we observed the significant conserved motif only in a subset of genes that were differentially expressed under P limitation or deficiency (Whitney & Lomas 2016, Bachy et al. 2018). Both the observed differences in the *psr*1-like gene and differences in associated binding motifs between the species may represent adaptation to distinct environments, as *M. pusilla* was collected in the temperate English Channel, while *M. commoda* was isolated from the tropics (Worden 2006).

The *psr*1-like gene in *M. commoda* and *M. pusilla* was one of the highest DE genes in each experiment (Whitney & Lomas 2016, Bachy et al. 2018), suggesting that this potential TF plays a critical role in the response of *Micromonas* to P deficiency. Moreover, the *psr*1-like gene was highly expressed in 2 culture experiments with different growth conditions and sampled at different growth stages, suggesting a broad physiological relevance for the Psr1-like TF (Fig. 6). In contrast to the transcriptome results, a recent study describing proteome changes in *M. pusilla* CCMP1545 grown under P-limited conditions in a bioreactor (Guo et al. 2018) did not observe sig-

nificant regulation of the Psr1-like protein (significance defined by Guo et al. 2018). The discordant results may be due to known differences in regulation between genes and proteins (Guo et al. 2018) or to different Psr1-like protein behavior under continuous culturing conditions. Regardless, these results warrant further investigation into the physiological role of the Psr1-like protein in *M. pusilla*.

The variable and non-uniform dynamics of several TCA cycle metabolites between treatments suggested that this pathway could be involved in the metabolic response to P deficiency in *M. pusilla*. Indeed, nearly all of the genes involved in the end of glycolysis and in the TCA cycle were up-regulated in *M. pusilla* (Bachy et al. 2018), and these genes contained the significant conserved motif. The gene encoding for fumarase, in particular, was upregulated in both *M. pusilla* and *M. commoda* transcriptomes under P limitation or deficiency. If fumarase gene expression is regulated by the Psr1-like protein, expression of these 2 genes (fumarase gene and *psr*1) should be correlated in field populations. We observed support for this hypothesis within the *Tara* Oceans dataset, but observed weaker relationships between *psr*1-like gene expression and other up-regulated genes in either *M. pusilla* or *M. commoda* (Text S3). In *M. pusilla*, carbon flow through the TCA cycle may increase as a means to fuel triacylglycerol (TAG) or starch production and to pull potentially damaging energy away from the photosystems (Norici et al. 2011, Klok et al. 2013). Similarly, several proteins involved in glycolysis (e.g. pyruvate dehydrogenase) and the TCA cycle (e.g. succinate dehydrogenase) were found to be up-regulated in another study with *M. pusilla* under P limitation (Guo et al. 2018), lending some support to our hypothesis that carbon flow through the TCA cycle increases under P deficiency. Insight from the latter study underscores potential differences between gene and enzyme regulation in glycolysis and the TCA cycle (Guo et al. 2018). For example, we found congruency in up- or down-regulation of some proteins from Guo et al. (2018) that we would expect in *M. pusilla* under P deficiency based on our combined comparative genomics and metabolomics approach (i.e. pyruvate kinase, pyruvate dehydrogenase, oxoglutarate dehydrogenase, and succinate dehydrogenase) but not others (i.e. fumarase, aconitase, citrate synthase). Analysis of transcript, protein, and metabolite responses in *M. pusilla* under the same growth conditions will be required to elucidate the role of a Psr1-like TF in this and other taxa.

In addition to TCA cycle intermediates, we observed shifts for several purine nucleosides between treatments and detected the significant conserved motif in genes for a nucleoside phosphatase and aspartate transcarbamylase. These results suggest increased nucleotide salvage through purine nucleotides and nucleosides, a mechanism described in *M. commoda* (Whitney & Lomas 2016) and in other phytoplankton (Dyhrman & Palenik 2003, Kujawinski et al. 2017). Previous phytoplankton work has also highlighted expression of the POX-encoding gene (Rokitta et al. 2014, 2016) in nutrient limitation experiments (including P deficiency) with the haptophyte *Emiliania huxleyi,* where this enzyme may have a role in stabilizing the mitochondrial membrane and in detecting cellular N levels. The POX gene was not present in *M. pusilla* but was up-regulated in *M. commoda* (Whitney & Lomas 2016; Table S4). Instead, in *M. pusilla*, a copper amine oxidase was up-regulated (Bachy et al. 2018) and contained the significant conserved motif that may function as a regulatory element for the Psr1-like TF. Thus, POX and copper amine oxidase represent gene targets for further investigation.

Maat et al. (2014) noted that both *E. huxleyi* (Borchard et al. 2011) and *M. pusilla* (Maat et al. 2014) exhibited a similar metabolic response to elevated pCO_2 levels and P-deficient conditions. While there may be multiple factors underlying the response of these organisms, both contain the *psr*1-like gene, which could direct part of a shared metabolic response to elevated pCO_2 and nutrient-limited conditions. While transcriptomic analysis of *E. huxleyi* was not performed by Borchard et al. (2011), Rokitta et al. (2014, 2016) performed microarray transcriptome analysis of *E. huxleyi* cells under separate N- and P-deficient conditions (normal pCO_2). The transcripts were only partial sequences; however, 2 up-regulated genes detected by Rokitta et al. (2016) contained myb-like DNA binding domains (gene IDs: GJ02872, GJ03978). Targeted experimental work, such as knockout or overexpression analysis (Bajhaiya et al. 2017), is necessary to elucidate the presence and role of a *psr*1-like gene in *E. huxleyi*. If there is a common role for the *psr*1-like gene in *E. huxleyi* and *M. pusilla* in their response to nutrient limitation and elevated pCO_2, this could have important implications for predicting the physiological response of the wide range of organisms that contain this *psr*1-like gene to changing environmental conditions.

The potential impact of Psr1-like regulated genes on the ecological roles of *Micromonas* spp. is unknown, but our results suggest that the Psr1-like protein coordinates a metabolic shift in these organisms under P

deficiency, altering the intracellular flow of carbon and other elements. More comprehensive examination of these metabolic responses, which likely vary to some extent among organisms, will be paramount to improving models of trophic carbon flow. More experiments are needed to characterize the structure and role of the *psr*1-like gene in *Micromonas* spp. and other phytoplankton, including: (1) confirming the presence of the *psr*1-like gene with genetic experiments, (2) determining the conditions under which the Psr1-like protein is abundant, (3) identifying the taxon-specific genes affected by the Psr1-like protein, (4) verifying the interaction of the Psr1-like protein with the hypothesized binding sites, and (5) comparing the genetic and metabolic responses to P deficiency between organisms containing the *psr*1-like gene and those that do not. Exploring the underlying biology of the *psr*1-like gene will facilitate mechanistic understanding of the complex metabolic response of these organisms to P limitation and will enhance our ecological and biogeochemical predictions.

Acknowledgements. We thank Krista Longnecker for performing the total organic carbon analysis and Matthew Johnson and Elizabeth Harvey for assistance with flow cytometry and fluorescence induction and relaxation analysis. This research was funded by the Gordon and Betty Moore Foundation through Grant GBMF3304 to E.B.K., and it was partially supported by a grant from the Simons Foundation (Award ID 509034 to E.B.K.).

LITERATURE CITED

Alipanah L, Winge P, Rohloff J, Najafi J, Brembu T, Bones AM (2018) Molecular adaptations to phosphorus deprivation and comparison with nitrogen deprivation responses in the diatom *Phaeodactylum tricornutum*. PLOS ONE 13(2):e0193335

Bachy C, Charlesworth CJ, Chan AM, Finke JF and others (2018) Transcriptional responses of the marine green alga *Micromonas pusilla* and an infecting prasinovirus under different phosphate conditions. Environ Microbiol 20:2898–2912

Bailey TL, Boden M, Buske FA, Frith M and others (2009) MEME Suite: tools for motif discovery and searching. Nucl Acid Res 37:W202–W208

Bajhaiya AK, Moreira JZ, Pittman JK (2017) Transcriptional engineering of microalgae: prospects for high-value chemicals. Trends Biotechnol 35:95–99

Barrett LW, Fletcher S, Wilton SD (2012) Regulation of eukaryotic gene expression by the untranslated gene regions and other non-coding elements. Cell Mol Life Sci 69:3613–3634

Benjamini Y, Hochberg Y (1995) Controlling the false discovery rate: a practical and powerful approach to multiple testing. J R Statist Soc B 57: 289–300

Berdalet E, Latasa M, Estrada M (1994) Effects of nitrogen and phosphorus starvation on nucleic acid and protein content of *Heterocapsa* sp. J Plankton Res 16:303–316

Borchard C, Borges AV, Haendel N, Engel A (2011) Biogeochemical response of *Emiliania huxleyi* (PML B92/11) to elevated CO_2 and temperature under phosphorous [sic] limitation: a chemostat study. J Exp Mar Biol Ecol 410: 61–71

Borneman AR, Gianoulis TA, Zhang ZD, Yu H and others (2007) Divergence of transcription factor binding sites across related yeast species. Science 317:815–819

Cañavate JP, Armada I, Hachero-Cruzado I (2017) Common and species-specific effects of phosphate on marine microalgae fatty acids shape their function in phytoplankton trophic ecology. Microb Ecol 74:623–639

Carradec Q, Pelletier E, Da Silva C, Alberti A and others (2018) A global ocean atlas of eukaryotic genes. Nat Commun 9:373

Chung CC, Hwang SPL, Chang J (2003) Identification of a high-affinity phosphate transporter gene in a prasinophyte alga, *Tetraselmis chui*, and its expression under nutrient limitation. Appl Environ Microbiol 69:754–759

De Carvalho CCCR, Fernandes P (2010) Production of metabolites as bacterial responses to the marine environment. Mar Drugs 8:705–727

Demory D, Arsenieff L, Simon N, Six C and others (2017) Temperature is a key factor in *Micromonas*–virus interactions. ISME J 11:601–612

Derelle E, Ferraz C, Rombauts S, Rouzé P and others (2006) Genome analysis of the smallest free-living eukaryote *Ostreococcus tauri* unveils many unique features. Proc Natl Acad Sci USA 103:11647–11652

Dittmar T, Koch B, Hertkorn N, Kattner G (2008) A simple and efficient method for the solid-phase extraction of dissolved organic matter (SPE-DOM) from seawater. Limnol Oceanogr Methods 6:230–235

Dyhrman ST, Palenik B (2003) Characterization of ectoenzyme activity and phosphate-regulated proteins in the coccolithophorid *Emiliania huxleyi*. J Plankton Res 25:1215–1225

Dyhrman ST, Ruttenberg KC (2006) Presence and regulation of alkaline phosphatase activity in eukaryotic phytoplankton from the coastal ocean: implications for dissolved organic phosphorus remineralization. Limnol Oceanogr 51:1381–1390

Dyhrman ST, Benitez-Nelson CR, Orchard ED, Haley ST, Pellechia PJ (2009) A microbial source of phosphonates in oligotrophic marine systems. Nat Geosci 2:696–699

Dyhrman ST, Jenkins DB, Rynearson TA, Saito MA and others (2012) The transcriptome and proteome of the diatom *Thalassiosira pseudonana* reveal a diverse phosphorus stress response. PLOS ONE 7:e33768

Edgar RC (2004) MUSCLE: multiple sequence alignment with high accuracy and high throughput. Nucleic Acids Res 32:1792–1797

Elser JJ, Bracken MES, Cleland EE, Gruner DS and others (2007) Global analysis of nitrogen and phosphorus limitation of primary producers in freshwater, marine and terrestrial ecosystems. Ecol Lett 10:1135–1142

Felsenstein J (1981) Evolutionary trees from DNA sequences: a maximum likelihood approach. J Mol Evol 17: 368–376

Feng TY, Yan ZK, Zheng JW, Xie Y and others (2015) Examination of metabolic responses to phosphorus limitation via proteomic analyses in the marine diatom *Phaeodactylum tricornutum*. Sci Rep 5:10373

Fiore CL, Longnecker K, Kido Soule MC, Kujawinski EB (2015) Release of ecologically relevant metabolites by

the cyanobacterium *Synechococcus elongatus* CCMP 1631. Environ Microbiol 17:3949–3963

Franco-Zorrilla JM, López-Vidriero I, Carrasco JL, Godoy M, Vera P, Solano R (2014) DNA-binding specificities of plant transcription factors and their potential to define target genes. Proc Natl Acad Sci USA 111:2367–2372

Goncalves EC, Johnson JV, Rathinasabapathi B (2013) Conversion of membrane lipid acyl groups to triacylglycerol and formation of lipid bodies upon nitrogen starvation in biofuel green algae *Chlorella* UTEX29. Planta 238: 895–906

Guo J, Wilken S, Jimenez V, Choi CJ and others (2018) Specialized proteomic responses and an ancient photoprotection mechanism sustain marine green algal growth during phosphate limitation. Nat Microbiol 3:781–790

Gupta S, Stamatoyannopolous JA, Bailey T, Noble WS (2007) Quantifying similarity between motifs. Genome Biol 8:R24

Halsey KH, Milligan AJ, Behrenfeld MJ (2014) Contrasting strategies of photosynthetic energy utilization drive lifestyle strategies in ecologically important picoeukaryotes. Metabolites 4:260–280

Hockin NL, Mock T, Mulholland F, Kopriva S, Malin G (2012) The response of diatom central carbon metabolism to nitrogen starvation is different from that of green algae and higher plants. Plant Physiol 158:299–312

Hoppe CJM, Flintrop CM, Rost B (2018) The Arctic picoeukaryote *Micromonas pusilla* benefits synergistically from warming and ocean acidification. Biogeosciences 15:4353–4365

Johnson LK, Alexander H, Brown CT (2019) Re-assembly, quality evaluation, and annotation of 678 microbial eukaryotic reference transcriptomes. GigaScience 8: giy158

Johnson WM, Kido Soule MC, Kujawinski EB (2017) Extraction efficiency and quantification of dissolved metabolites in targeted marine metabolomics. Limnol Oceanogr Methods 15:417–428

Jones DT, Taylor WR, Thornton JM (1992) The rapid generation of mutation data matrices from protein sequences. Comput Appl Biosci 8:275–282

Karl DM (2014) Microbially mediated transformations of phosphorus in the sea: new views of an old cycle. Annu Rev Mar Sci 6:279–337

Kido Soule MCK, Longnecker K, Johnson WM, Kujawinski EB (2015) Environmental metabolomics: analytical strategies. Mar Chem 177:374–387

Kishino H, Miyata T, Hasegawa M (1990) Maximum likelihood inference of protein phylogeny and the origin of chloroplasts. J Mol Evol 31:151–160

Klok AJ, Martens DE, Wijffels RH, Lamers PP (2013) Simultaneous growth and neutral lipid accumulation in microalgae. Bioresour Technol 134:233–243

Kujawinski EB, Longnecker K, Alexander H, Dyhrman ST, Fiore CL, Haley ST, Johnson WM (2017) Phosphorus availability regulates intracellular nucleotides in marine eukaryotic phytoplankton. Limnol Oceanogr Lett 2: 119–129

Kumar S, Stecher G, Tamura K (2016) MEGA7: Molecular Evolutionary Genetics Analysis version 7.0 for bigger datasets. Mol Biol Evol 33:1870–1874

Lai J, Yu Z, Song X, Cao X, Han X (2011) Responses of the growth and biochemical composition of *Prorocentrum donghaiense* to different nitrogen and phosphorus concentrations. J Exp Mar Biol Ecol 405:6–17

Li M, Shi X, Guo C, Lin S (2016) Phosphorus deficiency inhibits cell division but not growth in the dinoflagellate *Amphidinium carterae.* Front Microbiol 7:826

Li WKW (1994) Primary production of prochlorophytes, cyanobacteria, and eukaryotic ultraphytoplankton: measurements from flow cytometric sorting. Limnol Oceanogr 39:169–175

Lin S, Litaker RW, Sundra WG (2016) Phosphorus physiological ecology and molecular mechanisms in marine phytoplankton. J Phycol 52:10–36

Loebl M, Cockshutt AM, Campbell D, Finkel ZV (2010) Physiological basis for high resistance to photoinhibition under nitrogen depletion in *Emiliania huxleyi.* Limnol Oceanogr 55:2150–2160

Lomas MW, Swain A, Shelton R, Ammerman JW (2004) Taxonomic variability of phosphorus stress in Sargasso Sea phytoplankton. Limnol Oceanogr 49:2303–2309

Longnecker K (2015) Dissolved organic matter in newly formed sea ice and surface seawater. Geochim Cosmochim Acta 171:39–49

Maat DS, Crawfurd KJ, Timmermans KR, Brussaard CPD (2014) Elevated CO_2 and phosphate limitation favor *Micromonas pusilla* through stimulated growth and reduced viral impact. Appl Environ Microbiol 80: 3119–3127

Maat DS, van Bleijswijk JDL, Witte HJ, Brussaard PD (2016) Virus production in phosphorus-limited *Micromonas pusilla* stimulated by a supply of naturally low concentrations of different phosphorus sources, far into the lytic cycle. FEMS Microbiol Ecol 92:fiw136

Marchler-Bauer A, Bryant SH (2004) CD-Search: protein domain annotations on the fly. Nucleic Acids Res 32(Suppl 2):W327–W331

Markou G, Nerantzis E (2013) Microalgae for high-value compounds and biofuels production: a review with focus on cultivation under stress conditions. Biotechnol Adv 31:1532–1542

Martin P, Van Mooy BAS, Heithoff A, Dyhrman ST (2011) Phosphorus supply drives rapid turnover of membrane phospholipids in the diatom *Thalassiosira pseudonana.* ISME J 5:1057–1060

Martin P, Dyhrman ST, Lomas MW, Poulton NJ, Van Mooy BAS (2014) Accumulation and enhanced cycling of polyphosphate by Sargasso Sea phytoplankton in response to low phosphorus. Proc Natl Acad Sci USA 111:8089–8094

Martiny AC, Ustick L, Garcia CA, Lomas MW (2020) Genomic adaptation of marine phytoplankton populations regulates phosphate uptake. Limnol Oceanogr 65:S340–S350

Moseley JL, Chang CW, Grossman AR (2006) Genome-based approaches to understanding phosphorus deprivation responses and PSR1 control in *Chlamydomonas reinhardtii.* Eukaryot Cell 5:26–44

Müller R, Morant M, Jarmer H, Nilsson L, Nielsen TH (2007) Genome-wide analysis of the *Arabidopsis* leaf transcriptome reveals interaction of phosphate and sugar metabolism. Plant Physiol 143:156–171

Norici A, Bazonni AM, Pugnetti A, Raven JA, Giordano M (2011) Impact of irradiance on the C allocation in the coastal marine diatom *Skeletonema marinoi* Sarno and Zingone. Plant Cell Environ 34:1666–1677

Rengefors K, Ruttenberg KC, Haupert CL, Taylor C, Howes BL, Anderson DM (2003) Experimental investigation of taxon-specific response of alkaline phosphatase activity in natural freshwater phytoplankton. Limnol Oceanogr 48:1167–1175

Rokitta SD, von Dassow P, Rost B, John U (2014) *Emiliania huxleyi* endures N-limitation with an efficient metabolic budgeting and effective ATP synthesis. BMC Genomics 15:1051

Rokitta SD, von Dassow P, Rost B, John U (2016) P- and N-depletion trigger similar cellular responses to promote senescence in eukaryotic phytoplankton. Front Mar Sci 3:109

Rubio V, Linhares F, Solano R, Martín AC, Iglesias J, Leyva A, Paz-Ares J (2001) A conserved MYB transcription factor involved in phosphate starvation signaling both in vascular plants and in unicellular algae. Genes Dev 15: 2122–2133

Rusch DB, Halpern AL, Sutton G, Heidelberg KB and others (2007) The *Sorcerer II* global ocean sampling expedition: northwest Atlantic through eastern tropical Pacific. PLOS Biol 5:e77

Santos-Beneit F (2015) The Pho regulon: a huge regulatory network in bacteria. Front Microbiol 6:402

Shemi A, Schatz D, Fredricks HF, Van Mooy BAS, Porat Z, Vardi A (2016) Phosphorus starvation induces membrane remodeling and recycling in *Emiliania huxleyi.* New Phytol 211:886–898

Shi X, Lin X, Li L, Palenik B, Lin S (2017) Transcriptomic and microRNAomic profiling reveals multi-faceted mechanisms to cope with phosphate stress in a dinoflagellate. ISME J 11:2209–2218

Sosa OA, Caey JR, Karl DM (2019) Methylphosphonate oxidation in *Prochlorococcus* strain MIT9301 supports phosphate acquisition, formate excretion and carbon assimilation into purines. Appl Environ Microbiol 85: e00289-19

Tyrrell T (1999) The relative influences of nitrogen and phosphorus on oceanic primary production. Nature 400: 525–531

Van Mooy BAS, Fredricks HF, Pedler BE, Dyhrman ST and others (2009) Phytoplankton in the ocean use non-phosphorus lipids in response to phosphorus scarcity. Nature 458:69–72

Whitney LP, Lomas MW (2016) Growth on ATP elicits a P-stress response in the picoeukaryote *Micromonas pusilla.* PLOS ONE 11:e0155158

Worden AZ (2006) Picoeukaryote diversity in coastal waters of the Pacific Ocean. Aquat Microb Ecol 43: 165–175

Wykoff DD, Grossman AR, Weeks DP, Usuda H, Shimogawara K (1999) Psr1, a nuclear localized protein that regulates phosphorus metabolism in *Chlamydomonas.* Proc Natl Acad Sci USA 96:15336–15341

Editorial responsibility: Zoe Finkel, Sackville, New Brunswick, Canada
Reviewed by: 3 anonymous referees

Submitted: October 16, 2019
Accepted: November 10, 2020
Proofs received from author(s): February 11, 2021